JOURNAL OF PROPULSION AND POWER
Vol. 11, No. 6, November–December 1995

Two-Dimensional Numerical Model of Plasma Flow in a Hall Thruster

Kimiya Komurasaki*
Nagoya University, Chikusa-ku, Nagoya 464-01, Japan
and
Yoshihiro Arakawa†
University of Tokyo, Bunkyo-ku, Tokyo 113, Japan

Two-dimensional numerical model of plasma flow in a Hall thruster has been made to estimate analytically the ion-loss flux to the walls of an acceleration channel, and to obtain information about desirable configurations for good thruster performance. The model presented herein is comprised of an electron diffusion equation and an ion kinetic equation, which enables one to compute electrostatic potential contours and ion-beam trajectories. In the first step ion-production distribution was assumed. From the results it was found that electric-field distortion, which is a main cause of ion-loss to the channel walls, is induced not only due to the curvature of magnetic field lines, but also due to the radial nonuniformity of ion-production distribution. In the second step, the ion-production distribution was self-consistently determined by combining an energy conservation equation with the previous two basic equations. The results indicate that the shape of ion-production distribution largely changes with the magnetic field geometry, and hence, the field geometry significantly influences the ion-loss flux to the channel walls. The computed ion-loss fraction (a fraction of ions produced that are lost to the walls) ranges from 0.30 to 0.55, and shows good agreement with the measured values. Therefore, this model should be an effective tool in both the design and improvement of Hall thrusters.

Nomenclature

A = area of the channel exit
B = magnetic induction
D = electron diffusion coefficient
E = electric field
e = electronic charge
F = thrust
f = beam-ion energy distribution function
I_a = acceleration current
I_b = ion-beam current
I_e = electron current
I_p = ion-production current
J_e = electron current density
J_i = ion current density
k = Boltzmann constant
M = ion mass
m = electron mass
$\dot{m}$ = propellant mass flow rate
n = plasma density
q = ion-production rate
T_e = electron temperature
t = time
V = volume of an element
V_a = acceleration voltage
V_m = mean beam-ion energy
v = ion velocity
x = ion position
α = ion-loss fraction
β = ion-production coefficient
Γ_i = ion flux
γ = excitation coefficient
γ_T = thrust coefficient
ε = ionization energy
η_a = acceleration efficiency
η_E = beam energy efficiency
η_t = thrust efficiency
η_u = propellant utilization
θ = angle of magnetic field lines with respect to the axis
θ_b = beam-divergence angle
κ = heat conductivity
μ = electron mobility
ν = electron collision frequency
ϕ = space potential

Received April 5, 1994; revision received Feb. 10, 1995; accepted for publication Feb. 10, 1995.

*Assistant Professor, Department of Aerospace Engineering, Furocho. Member AIAA.

†Professor, Department of Aeronautics, 7-3-1 Hongo. Member AIAA.

I. Introduction

HALL thrusters have axisymmetric electrodes and an acceleration channel in which radial magnetic fields are applied to maintain a relatively high voltage between the anode and the cathode neutralizer, and ions generated in the channel are accelerated in the axial direction to produce thrust. A schematic diagram of a Hall thruster is shown in Fig. 1. Since the channel is filled with quasineutral plasma, there is no space-charge limited current, and hence, this type of thruster can offer much higher thrust density than conventional ion thrusters. With this characteristic, there has been a trend towards re-evaluating Hall thrusters in the U.S.[1,2] and Japan[3] since the 1980s. In addition, Russia has maintained a substantial research and development effort for over 30 years, and more than 50 of these thrusters have been utilized in space for stationkeeping of satellites.[4,5]

In our previous work on Hall thrusters,[6,7] thruster performance was improved through some modifications in thruster configuration: shortening the channel length together with arranging the magnetic field lines to be perpendicular to the axis. However, thrust efficiency was still low compared with that of conventional ion thrusters. From the measurement of the plasma properties inside the channel, the ion current lost to the channel walls was found to be considerably large, resulting in low thrust efficiency. In order to reduce the ion loss and to improve the thrust efficiency, an analytical approach

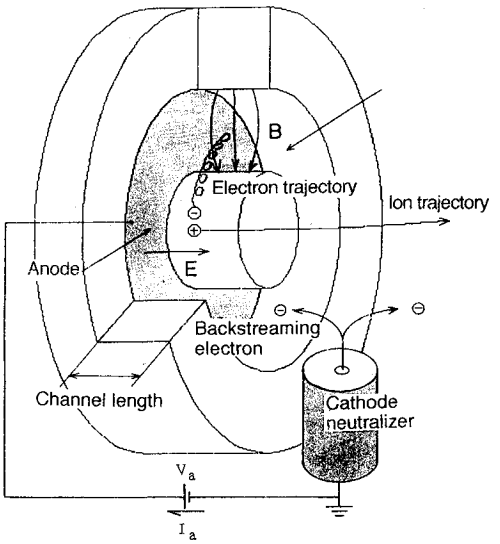

Fig. 1 Hall thruster schematic diagram.

was seen to be very effective when coupled with experimental efforts.

II. Numerical Model

In the design of Hall thrusters, the channel length is chosen to be larger than the electron cyclotron radius and to be smaller than the ion cyclotron radius, so that the applied magnetic field works preferentially on electrons, but not on ions. In addition, the ion mean free path is usually longer than the channel length, and the electron Hall parameter is much larger than unity in the channel, because the density is not as high as that in MPD thrusters. In these conditions, ions are electrostatically accelerated downstream without collisions, whereas electrons are constrained to azimuthal drift motions by the interaction with the radial magnetic field. However, axial electron current arises simultaneously from the classical or Bohm diffusion in the direction of the electric field.

The ionization process in a Hall thruster depends on its operational type. In the case of single-stage discharge operation, propellant gas is injected from the anode and ionized in the channel by the discharge between the anode and the cathode neutralizer. On the other hand, in the case of double-stage discharge operation,[3,8] a plasma source is located at the upstream end of the acceleration channel, and ions are produced there by a discharge independent of the main discharge.

A. Assumptions

This numerical model is based on the following assumptions. A steady-state, axisymmetric plasma flow of ions and of electrons in the acceleration channel is considered. Ions are electrostatically accelerated without collisions, while electrons diffuse in the axial and radial directions by electric fields and by density gradient. The diffusion coefficient across the magnetic field lines has a direct connection to the thruster performance. According to previous studies,[9-11] anomalous diffusion associated with electric-field oscillations has been observed in a transverse magnetic field. The diffusion coefficients deduced from these experiments varied inversely proportional to the magnetic induction. Therefore, Bohm diffusion[2,12] is assumed in the present calculation. Although the near-wall conductivity[13,14] would be another cause for such anomalous diffusion, it is not considered here because the effect on electric-field formation in the interwall region would be small.

The magnetic fields are applied by a magnetic circuit consisting of solenoidal coils and magnetic pole pieces. Induced magnetic fields by diamagnetic currents in the plasma are neglected, since plasma pressure is much smaller than magnetic field pressure in the acceleration channel.

B. Basic Equations

Ions are accelerated by electrostatic fields and the equation of motion is expressed as

$$M\frac{dv}{dt} = eE \tag{1}$$

As for electrons, the diffusion current density is expressed by

$$J_e = en[\mu]E + e[D]\nabla n \tag{2}$$

Note that this equation is concerned only with axial and radial electron motions, and not azimuthal ones. The electron mobility and the diffusion coefficient are expressed in tensors because these coefficients are anisotropic in the presence of magnetic fields. The coefficients parallel to magnetic field lines are expressed by the classical diffusion equations:

$$\mu_{\parallel} = e/m\nu, \qquad D_{\parallel} = kT_e/m\nu \tag{3}$$

The coefficients perpendicular to magnetic field lines are expressed by the Bohm diffusion relations:

$$\mu_{\perp} = 1/16B, \qquad D_{\perp} = kT_e/16eB \tag{4}$$

The mobility parallel to the field lines becomes four orders of magnitude larger than that perpendicular to the fields lines in the acceleration channel.

Ion and electron current conservation equations inside the channel are expressed by

$$\nabla\cdot J_i = eq \tag{5}$$

$$\nabla\cdot J_e = -eq \tag{6}$$

On the channel wall boundaries, the ions accelerated toward the channel walls are recombined with electrons. When the channel wall is nonconducting, the ion current to the wall surface must be equal to the electron current. Thereby, the boundary condition of current density on the wall surface becomes

$$(J_e)_n = -(J_i)_n \tag{7}$$

where $(J_e)_n$ and $(J_i)_n$ represent the electron and ion current density normal to the wall surface, respectively.

C. Ion Production

As for ion-production distribution, three cases are considered. In the first case, all ions are assumed to be produced in a plasma source located at the upstream end of the acceleration channel. Ions supplied by the plasma source are assumed to be introduced into the channel with the Bohm velocity, which is the boundary condition necessary to obtain the solution of monotonic decrease in space potential in the axial direction.[2] This case also corresponds to that of the sheath-type Hall thruster[15,16] in which ions are mostly produced in the thin sheath layer generated near the anode surface. On the other hand, in the case of single-stage discharge Hall thrusters, ion-production distribution spreads over the acceleration channel. Therefore, in the second case, the distribution of ion-production rate is assumed and the initial velocity of the produced ions is given as very small or zero.

In the third case, ion-production distribution is determined from the electron energy conservation equation instead of giving it as an input parameter for single-stage discharge Hall

thrusters. The electron energy conservation equation can be expressed as

$$\nabla\cdot[\tfrac{5}{2}kT_e(J_e/e)] = J_e\cdot E - (1+\gamma)\varepsilon\nabla\cdot J_e - \nabla\cdot[-n[\kappa]\nabla(kT_e)] \tag{8}$$

This equation indicates that the electrons gain energy by Joule heating and consume it in ionization and excitation in the channel. The last term on the right-hand side is associated with heat conduction. From the Reynolds analogy, heat conductivity is given as $[\kappa] = \frac{5}{2}[D]$. Substituting Eq. (6) into Eq. (8), the ion-production rate appears explicitly in the equation:

$$[(5kT_e/2e) + (1+\gamma)\varepsilon]q = J_e\cdot E - \tfrac{5}{2}J_e\cdot\nabla(kT_e/e) + \nabla\cdot[\tfrac{5}{2}n[D]\nabla(kT_e/e)] \tag{9}$$

Since the electron temperature variation in the channel is usually much smaller than that of the space potential (i.e., E), the temperature gradient term $\nabla(kT_e/e)$ is neglected here, and Eq. (9) reduces to

$$q = \frac{J_e\cdot E}{(5kT_e/2e) + (1+\gamma)\varepsilon} \tag{10}$$

Here, electron temperature is assumed identical to 10 eV, which is a typical value measured with electrostatic probes.[6,7] Ionization energy is 15.76 eV for argon gas and 12.13 eV for xenon gas, and the excitation coefficient is chosen as 2 according to Ref. 17. Although the absolute value of the ion-production rate changes with these parameters, it varies in proportion to the Joule heating distribution, and these parameters have little influence on the shape of the electric field and on the ion-loss fraction.

III. Calculation Procedure

There are two different parts to the calculation: the electron diffusion calculation and the ion trajectory calculation. In order to apply the finite element method to the electron diffusion calculation, the region inside the channel is divided into small triangular elements. The grid points are uniformly spaced in an x-y coordinate system, and the same grid system is also utilized for the ion trajectory calculation.

In the ion trajectory calculation, the ion flux produced in the kth element is given by

$$\Gamma_i^{(k)} = q^{(k)}V^{(k)} \tag{11}$$

where $q^{(k)}$ is the ion-production rate at the kth element and $V^{(k)}$ is its volume. When the space potential distribution is known, one can trace the ion trajectory by integrating Eq. (1), which is transformed to the following equations:

$$v_n = v_{n-1} + (eE/M)\Delta t \tag{12}$$

$$x_n = x_{n-1} + v_{n-1}\Delta t + (eE/2M)(\Delta t)^2 \tag{13}$$

Here, v_n and x_n denote the ion velocity and position vector at the nth iteration. Electric field is given as the gradient of space potential distribution

$$E = -\nabla\phi \tag{14}$$

Plasma density can be calculated by counting the number of ions passing through an element and their residence time in the element. The density at the lth element $n^{(l)}$ is given by

$$n^{(l)} = \sum_{k=l}^{N}\frac{\Gamma_i^{(k)}t^{(k,l)}}{V^{(l)}} \tag{15}$$

Here, $t^{(k,l)}$ represents the residence time of the respective ions in flux $\Gamma_i^{(k)}$ to stay in the lth element. The distribution of ion current lost on the wall surface is obtained by summing the ion flux arriving at the wall:

$$(J_i)_n^{(l)} = e\sum_{\text{wall}}\Gamma_i^{(k)}/S^{(l)} \tag{16}$$

Here, $(J_i)_n^{(l)}$ is the ion current density normal to the lth wall surface element and $S^{(l)}$ is its surface area.

Space potential distribution is obtained by solving the electron diffusion equation, which is rewritten by combining Eqs. (2), (6), and (14).

$$\nabla(n[\mu]\nabla\phi) = \nabla[D]\nabla n + q \tag{17}$$

Here, the tensors of electron mobility and diffusion coefficient are expressed as

$$[\mu] = [\Theta]^{-1}\begin{bmatrix}\mu_\perp & 0\\ 0 & \mu_\parallel\end{bmatrix}[\Theta],\quad [D] = [\Theta]^{-1}\begin{bmatrix}D_\perp & 0\\ 0 & D_\parallel\end{bmatrix}[\Theta] \tag{18}$$

at the point where the magnetic field line makes an angle of θ relative to the axis. The rotation matrix $[\Theta]$ is defined as

$$[\Theta] = \begin{bmatrix}\cos\theta & -\sin\theta\\ \sin\theta & \cos\theta\end{bmatrix} \tag{19}$$

The magnetic field is calculated prior to this analysis as a solution to the magnetostatic equations.

The boundary conditions of the space potential at the entrance and the exit of the channel are given as equal to the anode potential ϕ_{anode} at the entrance, and to zero at the exit:

$$\phi|_{\text{entrance}} = \phi_{\text{anode}},\qquad \phi|_{\text{exit}} = 0 \tag{20}$$

The calculation sequence is illustrated in Fig. 2. At the beginning of the calculation, channel geometry, and magnetic field configuration are given as input parameters. The ion-production distribution is, as previously mentioned, assumed in the first and the second cases, and is self-consistently calculated in the third case. Assuming the initial space potential distribution, one can calculate the ion trajectories from Eqs. (12) and (13). The plasma density and ion-loss distributions are obtained from Eqs. (15) and (16), respectively. With these distribution profiles, the electron diffusion equation, Eq. (17) is solved under the boundary conditions given by Eqs. (7) and (20), and the space potential is renewed. In the third case, ion-production distribution is determined by solving Eq. (10) with the calculated space potential and plasma density distributions. These calculations are repeated by turns until both space potential and plasma density are converged within tolerable error. Finally, the ion-loss fraction is evaluated by dividing the total ion-loss current by total ion-production current.

IV. Results and Discussion

For the first case with all ions produced at the channel entrance, two patterns of magnetic field configurations are considered and are shown in Fig. 3. In pattern I, the magnetic field lines are curved, becoming purely axial in the middle of the channel, while in pattern II, the magnetic field lines are predominantly in the radial direction. For checking the mesh-convergence, we used grids ranging from 8×40 to 32×160 for pattern I, and from 12×16 to 48×64 for pattern II.

As seen in the space potential profile in pattern I, the equipotential lines are curved in accordance with the magnetic field lines. This is because electrons move freely along the magnetic field lines rather than across them and eliminate the

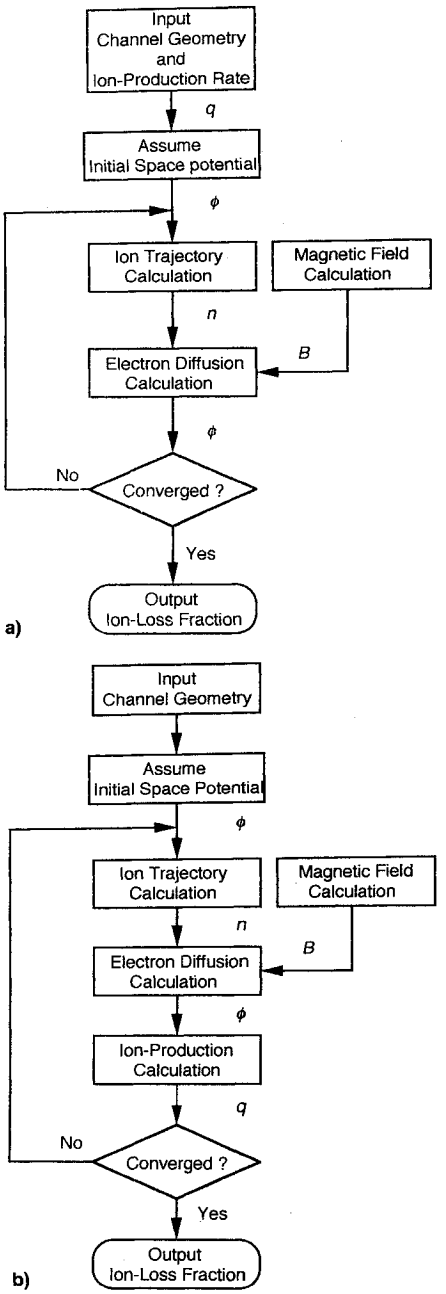

Fig. 2 Calculation sequence of two-dimensional plasma flow analysis with a) assumed ion-production rate and b) ion-production calculation.

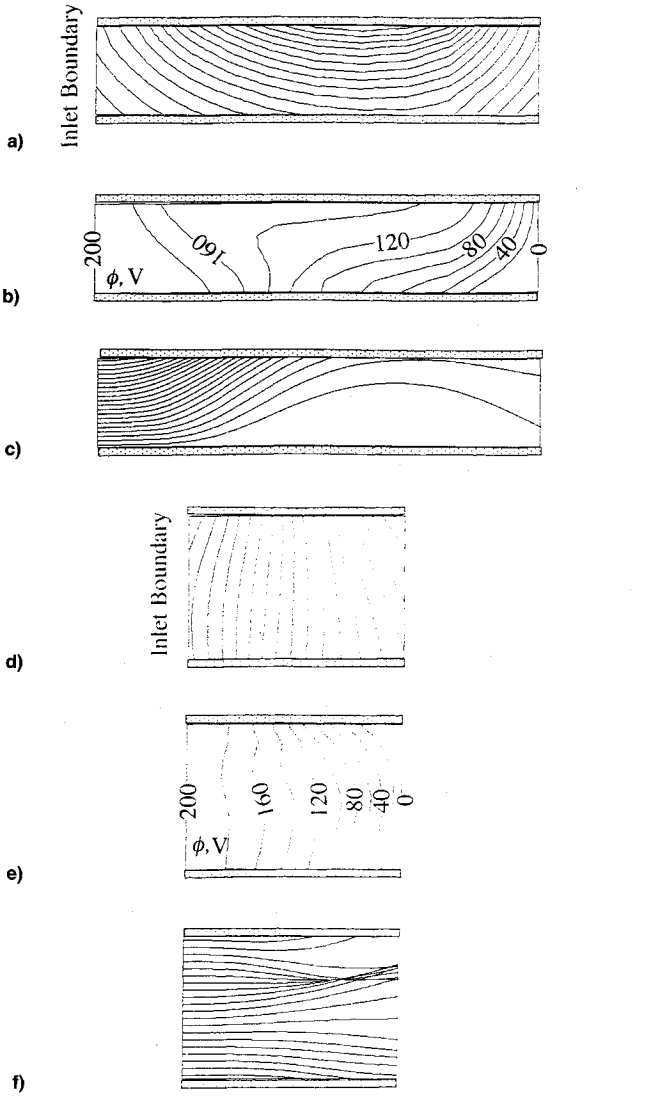

Fig. 3 Calculated distributions in the acceleration channel for double-stage discharge Hall thruster: propellant gas is argon. kT_e = 10 eV. Ion-current density on the inlet boundary is assumed 80 mA/cm²: a) magnetic field, pattern I; b) space potential; c) ion trajectory; d) magnetic field pattern II; e) space potential; and f) ion trajectory.

potential difference along them. As a result, a radial component of electric field is induced. Owing to this field distortion, most of the ions introduced into the channel are accelerated toward the outer wall and the ion-loss fraction exceeds 0.9. In the case of pattern II, the electric fields are mostly formed in the axial direction, and the ion-loss fraction becomes as small as 0.1. Such a large reduction in ion-loss fraction is mainly due to the better arrangement of the magnetic field lines that are formed almost perpendicular to the axis. Consequently, the electric field distortion, which is the cause of ion-loss to the channel walls, is found to be induced by the curved configuration of the magnetic field lines.

With an increase in magnetic induction, the space potential distribution hardly changes, and therefore, the ion-loss fraction remains almost constant for both cases. In contrast, backstreaming electron current is inversely proportional to the magnetic induction. As a result, the ratio between the beam-ion and the discharge currents increases with an increase in magnetic induction.

For the second case of an assumed distribution, the ion-production rate is assumed to have a peak in the middle of the channel as shown in Fig. 4. This distribution simulates the measured profile in the experiment.[7] A grid system of 24 × 32, which corresponds to Δx = 0.25 mm, and 1024 macroparticles/mm² are used.

Calculated plasma properties are also shown in Fig. 4. As seen in the space potential profile, axial electric fields dominate in the channel. However, a radial component of the electric field is induced in the regions near the wall surfaces. The polarity of this component retards the electron flux toward the wall, and is balanced by flux toward the wall produced by the density gradient, since the electron flux to the wall is small due to the boundary condition [see Eqs. (2) and (7)]. This field distortion (Fig. 4c) is also observed in the experiment. The ions produced near the walls are accelerated toward the walls by the radial electric field, and the ion-loss fraction becomes 0.25. As the electron temperature increases, the electron diffusion coefficient becomes larger and the density gradient effect stronger, and consequently, the ion loss increases.

The radial density gradient, which produces the electric-field distortion, is thought to come from the radial gradient

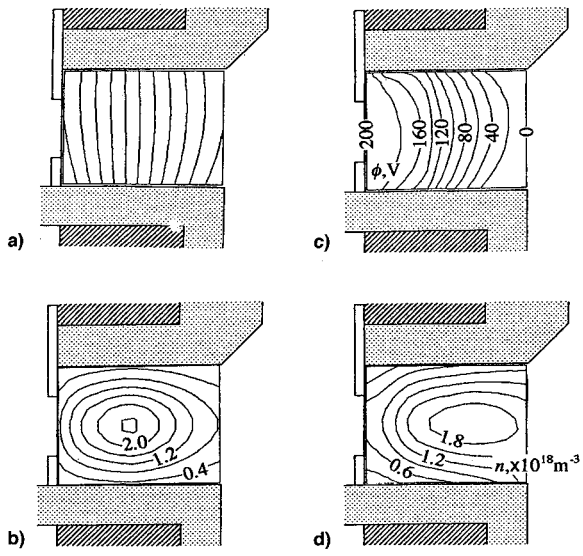

Fig. 4 Calculated distributions in the acceleration channel for single-stage discharge Hall thruster: propellant gas is argon. kT_e = 10 eV. Ion-production rate is normalized: a) magnetic field, b) ion-production rate (assumed), c) space potential, and d) plasma density.

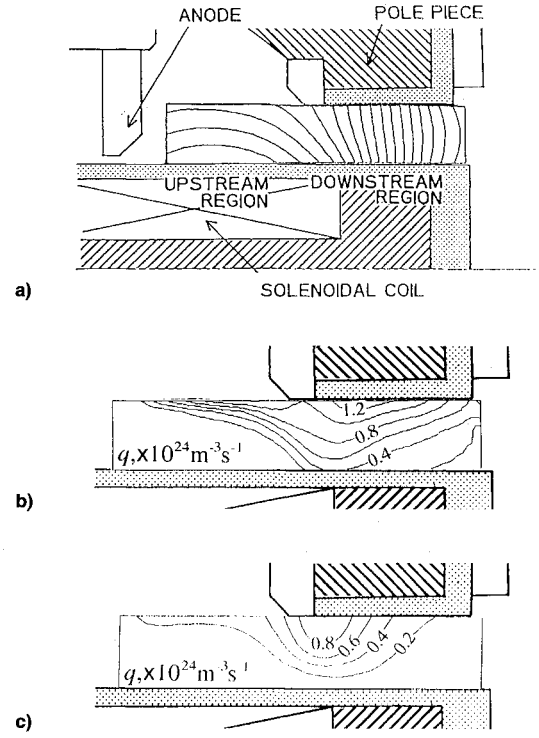

Fig. 5 Calculated and measured distributions in the acceleration channel of thruster I: propellant gas is argon. kT_e = 10 eV and q = 4 × 10^{23} $m^{-3}s^{-1}$ are assumed in calculation: a) thruster I, b) ion-production rate (calculated), and c) ion-production rate (measured).

of ion-production rate. In the case where the ion-production distribution is assumed radially uniform, plasma density also becomes uniform, and hence no radial electric field is induced, resulting in a low ion-loss fraction of 0.06. In practice, it is, however, difficult to obtain a radially uniform distribution of the ion-production rate, and therefore, there is an optimum magnetic field configuration which cancels the effect of the ion-production gradient.

In the third case [Eq. (9)], calculation was conducted on two different Hall thrusters, and the results are compared with the measured ones. Thruster I was constructed at the University of Tokyo[6] and thruster II was developed at the

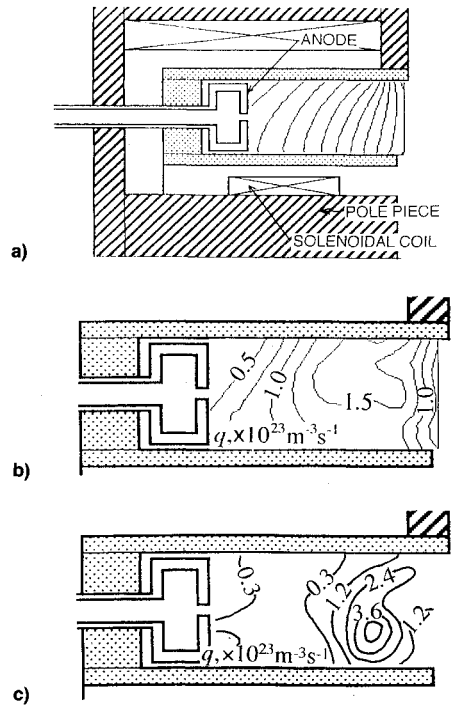

Fig. 6 Calculated and measured distributions in the acceleration channel of thruster II: propellant gas is xenon. kT_e = 10 eV and q = 1 × 10^{23} $m^{-3}s^{-1}$ are assumed in calculation: a) thruster II, b) ion-production rate (calculated), and c) ion-production rate (measured).

Moscow Aviation Institute in Russia.[18] Previously, these thrusters had been experimentally investigated, and the plasma properties' profiles in the channel were measured with electrostatic probes. The computed results for thruster I and for thruster II are shown in Figs. 5 and 6, respectively. As seen in Fig. 5, the ion-production distribution has a peak in the region very close to the outer wall, and half of the ions produced there are lost to the outer wall, resulting in a high ion-loss fraction of 0.55.

In the case of thruster II, the calculated ion-loss fraction becomes 0.3. This value is about half of that of thruster I. As seen in Fig. 6, the ion-production distribution is not biased toward the outer wall, but has a peak in the center region of the channel. This is because the electron current density near the outer wall is relatively low (thereby, the production rate is small) due to the high magnetic induction and low electron mobility. However, the peak of the ion-production rate shifts to the downstream region, where strong electric fields are induced. With this ion-production distribution, the ions are extracted from the channel exit with a relatively low ion-loss fraction. Such a magnetic field configuration (high magnetic induction near the exit) is a distinctive feature of the conventional Russian Hall thrusters. The computed profiles of the ion-production distribution show good agreement with the measured ones.

Finally, the relationship between the ion-loss fraction and thruster performance is discussed. From a simple plasma discharge model (see Appendix), one can rewrite the acceleration efficiency (the ratio of ion-beam current to acceleration current) in terms of the ion-loss fraction and the ion-production coefficient as

$$\eta_a = \frac{1}{1 + [1/\beta(1 - \alpha)]} \tag{21}$$

Here, the ion-production coefficient is approximated from Eq. (10) as

$$\beta = \frac{V_a}{(5kT_e/2e) + (1 + \gamma)\varepsilon} \tag{22}$$

Equation (21) implies that high acceleration efficiency is obtained with low ion-loss fraction and with high ion-production coefficient. As previously shown in this article, ion-loss fraction changes from 0.1 to 0.9 depending on the thruster configuration. On the other hand, the ion-production coefficient is, as seen in Eq. (22), dependent on the operational parameters, and not on the geometrical parameters of the thruster configuration.

The thrust efficiency is expressed as a product of three internal efficiencies (see Appendix); acceleration efficiency, propellant utilization and beam energy efficiency:

$$\eta_T \approx \eta_a \eta_u \eta_E \tag{23}$$

Among these internal efficiencies, the acceleration efficiency is usually the lowest one and is a key parameter for performance improvement. Therefore, the improvement of the acceleration efficiency by reducing the ion-loss fraction is the most effective way to achieve high thrust efficiency.

V. Summary

A two-dimensional plasma flow model, which is comprised of an electron diffusion equation and an ion kinetic equation, has been made to compute ion-loss flux to the surrounding walls of an acceleration channel.

In the first step, the distributions of plasma properties such as space potential, plasma density and ion-loss rate are calculated, and the ion-loss fraction is estimated. As a result, it was found that the radial electric field, which is a main cause of ion-loss to the walls, is induced both by the radial gradient of ion-production distribution and by the curvature of the magnetic field lines. Therefore, channel geometry and magnetic field configuration should be determined after consideration of the influence of ion-production distribution on ion-loss flux to the walls.

In the second step, ion-production distribution was self-consistently determined from the energy conservation equation coupled with the above equations. The results indicate that the ion-production distribution changes largely with the magnetic induction distribution, and hence, the magnetic field configuration is found to have a great influence on the ion-loss fraction and on the thruster performance. The calculated results were compared with the measured ones, and have shown good agreement. From this fact, it was concluded that this model is a useful tool for estimation of ion-loss fraction in the acceleration channel.

Appendix: Definition of the Efficiencies

From a thrust measurement, one can calculate thrust efficiency using the well-known relation as given by

$$\eta_t = (F^2/2\dot{m}V_aI_a) \tag{A1}$$

Neither excitation power for solenoidal coils nor heating power for a cathode neutralizer is taken into account in the calculation of thrust efficiency, since they are much smaller than the power for main discharge.

In order to investigate thruster performance characteristics, the following internal efficiencies are introduced and defined by the equations:

$$\eta_a = (I_b/I_a) \tag{A2}$$

$$\eta_u = (MI_b/e\dot{m}) \tag{A3}$$

$$\eta_E = (V_m/V_a) \tag{A4}$$

Here, V_m is the mean beam-ion energy which is calculated from the ion-energy distribution as

$$V_m = \left[\int f(V)\sqrt{V}\,dV\right]^2 \tag{A5}$$

When all ions are singly charged and are accelerated only in the axial direction, thrust can be written by

$$F = I_b\sqrt{2MV_m/e} \tag{A6}$$

Considering the exhaust-beam divergence and the electron pressure contribution to the thrust, it can be rewritten as

$$F = I_b\sqrt{2MV_m/e}\cos\theta_b + AnkT_e = \gamma_T I_b\sqrt{2MV_m/e} \tag{A7}$$

where γ_T is defined as

$$\gamma_T = \cos\theta_b + kT_e/eV_m \tag{A8}$$

While the internal efficiencies vary widely with operational conditions, γ_T remains approximately unity. Substituting Eqs. (A2–A4) and (A7) into Eq. (A1), the thrust efficiency yields

$$\eta_T = \gamma_T^2\eta_a\eta_u\eta_E \approx \eta_a\eta_u\eta_E \tag{A9}$$

Typical examples of such internal efficiencies and thrust efficiency for several operating conditions are listed in Table A1. As seen in this table, the acceleration efficiency is the most predominant factor for determining thrust efficiency.

To evaluate the acceleration efficiency in detail, a simple model is presented as follows. In the acceleration channel, ions are produced by ionization collisions of electrons with neutral atoms, and total ion-production current in the channel can be expressed by

$$I_p = \beta I_e \tag{A10}$$

where I_e is electron current backstreaming from the cathode to the anode and a coefficient β is a quantity that expresses how efficiently ions are produced. Since the volume recombination in the channel can be neglected, the ions produced are either lost to the channel walls or exhausted downstream from the exit. Thereby, I_b is given by

$$I_b = (1 - \alpha)I_p \tag{A11}$$

where α denotes a fraction of ions produced that are lost to the walls.

The sum of the ion-beam current and the electron current is equal to the acceleration current as

$$I_a = I_b + I_e \tag{A12}$$

Substituting Eqs. (A10–A12) into Eq. (A2), the acceleration efficiency can be expressed as a function of α and β as

$$\eta_a = \frac{1}{1 + 1/\beta(1 - \alpha)} \tag{A13}$$

This equation indicates that, in order to obtain a high acceleration efficiency, the ion loss fraction should be as low as possible, together with highly efficient ion production.

Table A1 Typical operating parameters and efficiencies[6]

$\dot{m}$, A-eq.	V_a, V	I_a, A	I_b, A	η_a, %	η_u, %	η_E, %	η_t, %
0.30	150	0.82	0.23	28	77	66	14
0.50	100	1.49	0.37	25	74	65	12
0.50	130	1.40	0.38	27	76	65	13
0.50	150	1.45	0.40	28	80	62	14
0.70	150	2.21	0.65	29	97	62	17

Propellant gas is xenon.

References

[1]Plank, G. M., Kaufman, H. R., and Robinson, R. S., "Experimental Investigation of a Hall-Current Accelerator," AIAA Paper 82-1920, Nov. 1982.

[2]Kaufman, H. R., "Theory of Ion Acceleration with Closed Electron Drift," *Journal of Spacecraft and Rockets*, Vol. 21, No. 6, 1984, pp. 558–562.

[3]Yamagiwa, Y., and Kuriki, K., "Performance of Double-Stage-Discharge Hall Ion Thruster," *Journal of Propulsion and Power*, Vol. 7, No. 1, 1991, pp. 65–70.

[4]Bugrova, A. I., Kim, V., Maslennikov, N. A., and Morozov, A. I., "Physical Processes and Characteristics of Stationary Plasma Thrusters with Closed Electrons Drift," *Proceedings of the 22nd International Electric Propulsion Conference* (Viareggio, Italy), 1991 (IEPC 91-079).

[5]Barnett, J. W., "A Review of Soviet Plasma Engine Development," AIAA Paper 90-2600 (Orlando, FL), 1990.

[6]Komurasaki, K., and Arakawa, Y., "Hall Current Ion Thruster Performance," *Journal of Propulsion and Power*, Vol. 8, No. 6, 1992, pp. 1212–1216.

[7]Komurasaki, K., Hirakawa, M., and Arakawa, Y., "Plasma Acceleration Process in a Hall-Current Thruster," *Proceedings of the 22nd International Electric Propulsion Conference* (Viareggio, Italy), 1991 (IEPC 91-078).

[8]Koehne, R., Linder, F., Schreitmueller, K. R., Wickmann, H. G., and Zeyfang, E., "Further Investigations on Low-Density Hall Accelerator," *AIAA Journal*, Vol. 8, No. 5, 1970, pp. 873–879.

[9]Janes G. S., and Lowder, R. S., "Anomalous Electron Diffusion and Ion Acceleration in a Low-Density Plasma," *Physics of Fluids*, Vol. 9, No. 6, 1966, pp. 1115–1123.

[10]Morozov, A. I., Esipchuk, Yu. V., Kapulkin, A. M., Nevrovskii, V. A., and Smirnov, V. A., "Azimuthally Asymmetric Modes and Anomalous Conductivity in Closed Electron Drift Accelerators," *Soviet Physics—Technical Physics*, Vol. 18, No. 5, 1973, pp. 615–620.

[11]Tilinin, G. N., "High Frequency Plasma Waves in a Hall Accelerator with an Extended Accelerator Zone," *Soviet Physics—Technical Physics*, Vol. 22, No. 8, 1977, pp. 974–978.

[12]Kaufman, H. R., and Robinson, R. S., "Plasma Processes in Inert-Gas Thrusters," *Journal of Spacecraft and Rockets*, Vol. 18, No. 5, 1981, pp. 470–476.

[13]Bugrova, A. I., Morozov, A. I., and Kharachevnikov, V. K., "Wall-Conductivity Effects in the Channel of a Closed-Drift-Circuit Plasma Accelerator," *Soviet Technical Physics Letters*, Vol. 9, No. 1, 1983, pp. 1, 2.

[14]Morozov, A. I., and Shubin, A. P., "Electron Kinetics in the Wall-Conductivity Regime: I and II," *Soviet Journal of Plasma Physics*, Vol. 10, No. 6, 1984, pp. 728–735.

[15]Brown, C. O., and Pinsley, E. A., "Further Experimental Investigations of a Cesium Hall-Current Accelerator," *AIAA Journal*, Vol. 3, No. 5, 1965, pp. 853–859.

[16]Zharinov, A. V., and Popov, Yu. S., "Acceleration of Plasma by a Closed Hall Current," *Soviet Physics—Technical Physics*, Vol. 12, 1967, pp. 208–211.

[17]Smirnov, V. A., "Electron Energy Balance in a Hall-Current Accelerator with an Extended Acceleration Zone," *Soviet Journal of Plasma Physics*, Vol. 5, No. 2, 1979, pp. 202–205.

[18]Bishaev, A. M., and Kim, V., "Local Plasma Properties in a Hall-Current Accelerator with an Extended Acceleration Zone," *Soviet Physics—Technical Physics*, Vol. 23, No. 9, 1978, pp. 1055–1057.